Geoderma 376 (2020) 114561

Contents lists available at ScienceDirect

Geoderma

journal homepage: www.elsevier.com/locate/geoderma

Structural alterations of synthetic allophane under acidic conditions: Implications for understanding the acidification of allophanic Andosols

Shun Wang[a,b], Peixin Du[a,b], Peng Yuan[a,b,*], Yaqi Liu[a,b], Hongzhe Song[a,b], Junming Zhou[a,b], Liangliang Deng[a,b], Dong Liu[a,b]

[a] CAS Key Laboratory of Mineralogy and Metallogeny/Guangdong Provincial Key Laboratory of Mineral Physics and Materials, Guangzhou Institute of Geochemistry, Institutions of Earth Science, Chinese Academy of Sciences, 511 Kehua Street, Guangzhou 510640, China
[b] University of Chinese Academy of Sciences, 19 Yuquan Road, Beijing 100049, China

ARTICLE INFO

Keywords:
Allophanic andosols
Acidification
Hydrous aluminosilicate
Allophane
Hollow spherical structure
Porosity

ABSTRACT

Acidification of allophanic Andosols has significant effects on their physicochemical properties and productivity. Understanding of the acidification and related effects is limited by the structural changes of allophane – the major mineral composition of allophanic Andosols. In this work, we systematically investigated the structural stability of allophane and the mechanisms of structural changes under different acidic conditions (initial pH 4.0–2.0) by using chemical analysis, transmission electron microscopy, X-ray diffraction, Fourier-transform infrared spectroscopy, solid-state magic-angle-spinning nuclear magnetic resonance, and N_2 physisorption analysis. The results indicated that the structure of allophane was readily altered in acidic conditions. Acid leaching in conditions with initial pH $>$ 3.0 only dissolved some polymerized silicates from allophane, enlarging the defect pores. By contrast, the dissolution of the imogolite-like local structure was observed in strongly acidic conditions (initial pH $<$ 3.0) and released large amounts of Al and Si, which can further enlarge defect pores or even make hollow spherules collapse followed by the precipitation of amorphous silica. As a result, the microporous parameters increased, reaching maxima in $Allo_{2.2}$, while the total porosity and specific surface area of products decreased with the decrease of initial pH of the leaching solutions. These changes are supposed to diminish the adsorption and storage capacities of guest species of allophane. These findings suggest that the rapid responsiveness of allophane to acid supposedly plays a crucial role in the acid buffering capacity of allophanic Andosols and that the structural destruction of allophane may significantly contribute to Al toxicity and to breaking the porous structure of acidified allophanic Andosols. For the management of allophanic Andosols, prudent measures should be taken to protect the allophane structure. And it is possible to restore the soil productivity of weakly acidified allophanic Andosols through soil remediation.

1. Introduction

Allophanic Andosols generally develop from volcanic parent materials and are characterized by a large content of allophane – a poorly crystalline hydrous aluminosilicate mineral with a varied chemical composition ($1–2SiO_2{\cdot}Al_2O_3{\cdot}5–6H_2O$) (Dahlgren et al., 2004; Du et al., 2018). The content of allophane in allophanic Andosols reaches up to 60 wt% (Stevens and Vucetich, 1985). Allophanic Andosols cover only about 1% of the Earth's land surface but represent an important land resource, as indicated by their high human carrying capacity of approximately 10% of the world's population (Gonzalez-Rodriguez and Fernandez-Marcos, 2018). This is due to the excellent tilth and high agricultural productivity of allophanic Andosols, which have been recognized as one of the most fertile soils in the world. These features are closely related to their peculiar chemical characteristics (e.g., low Al toxicity, abundant variable charge, and high cations, anions, and soil organic carbon contents) and physical properties (e.g., low bulk density (0.2–0.9 g/m^2) with high porosity and high specific surface area, high water retention, highly stable soil aggregates, and high resilience to compaction and erosion) (Shoji et al., 1993; Dahlgren et al., 2004; Parfitt, 2009; Filimonova et al., 2016).

The above-mentioned favorable properties of allophanic Andosols are largely attributed to the presence of allophane, whose unique structure and properties play a crucial role (Harsh et al., 2002; Levard et al., 2012, 2016; Filimonova et al., 2016). Specifically, allophane has a hollow spherical nanostructure and exhibits an external diameter of

* Corresponding author.
E-mail address: yuanpeng@gig.ac.cn (P. Yuan).

https://doi.org/10.1016/j.geoderma.2020.114561
Received 24 March 2020; Received in revised form 13 June 2020; Accepted 26 June 2020
Available online 06 July 2020

3.5–5 nm. The spherule wall contains several defect pores (0.35–0.5 nm) and is comprised of a curved gibbsite-like sheet with isolated/polymerized orthosilicate groups attached to its inside. On account of these features, allophane exhibits a high specific surface area (*SSA*, 300–500 m^2/g, theoretically up to ~1000 m^2/g) (Ohashi et al., 2002; Montarges-Pelletier et al., 2005; Abidin et al., 2006), with widespread hydroxyl groups (Si-OH and Al-OH) on the surface and near the defect edges (Khan et al., 2006; Levard et al., 2012). As a result, allophane-rich Andosols are endowed with properties such as high SSA and abundant variable surface charge as stated above, and they also have a high capacity for the adsorption of guest species (such as metal cations, anions, and soil organic carbon) through specific or non-specific adsorption mechanisms (Wada et al., 1989; Dahlgren et al., 2004; Harsh, 2012; Levard et al., 2016). For example, soil organic matter (SOM) can be strongly adsorbed to the surface of allophane spherules through ligand exchange between their carboxyl groups and the aluminol groups of allophane (Parfitt et al., 1999). Such complexation interactions are the key to the accumulation of SOM in allophanic Andosols as well as to the chemical protection of SOM against microbial decomposition (Kelliher et al., 2013; Pereira et al., 2019). The total carbon contents of allophanic Andosols are nearly 100% greater than those of non-allophanic counterparts (Kelliher et al., 2013), and even 3–6-fold higher than those of other kinds of soils containing classical clays (Woignier et al., 2015). In soils, allophane is readily formed and precipitated where sufficient Si and Al exist in solutions (Parfitt and Kimble, 1989; Parfitt, 2009); recently, Li et al (2020) reported that the rate of the formation of allophane could be up to 0.85 g kg^{-1} day^{-1}. Moreover, allophane particles are prone to form highly porous microaggregates. These features are highly responsible for the high porosity and low bulk density of allophanic Andosols (Henmi and Wada, 1976; Harsh et al., 2002). The bulk density of allophanic Andosol can be < 0.9 g/cm^3 when its allophane content is > 5% (Nanzyo et al., 1993). The porous structure of allophanic Andosols is further responsible for their high storage and retention capacities of water and nutrients, high permeability, and other desirable properties aforementioned (Nanzyo et al., 1993; Dahlgren et al., 2004; Chevallier et al., 2010), corresponding to their good performance in supporting vigorous plant growth and their capability of providing a conducive environment for deep rooting. Therefore, a good understanding of the structure and properties of allophane constitutes a base for understanding the properties of allophanic Andosols and related uses such as optimal management.

The acidification of allophanic Andosols is prevalent in nature. The process usually occurs slowly. However, acidification can be accelerated by anthropogenic or natural disturbances (Delmelle et al., 2001; Tao et al., 2019). In the case of allophanic Andosols under managed farming systems, human activities, especially the heavy application of fertilizers, can make the pH values of soil solutions in < 4.0 (Pansombat et al., 1997; Matsuyama et al., 2005; Takahashi et al., 2008). As stated by Guo et al. (2010), 50 kg/hectare of added ammonium-N fertilizer will generate hydrogen ions (H^+) of about 4 kilomole/hectare/year, and consumption of basic cations that results from the improved crop production can contribute a further amount of H^+ to the local environment. Another scenario that acidification of allophanic Andosols occurs is a location near active volcanoes, where the allophanic Andosols receive large inputs of acid compounds during and after each eruption. As a result, the pH value of rainwater can be as low as 2.5 in these regions (Johnson and Parnell, 1986; Herre et al., 2007).

Due to the serious threat of acidification to agricultural production and biodiversity in terrestrial ecosystems, the effects of acid inputs on allophanic Andosols have received increasing attention over the past decades. Previous studies have mainly focused on the effects of acidification on soil chemistry (e.g., pH, CEC, and acid-neutralizing capacity) (Takamatsu et al., 1992; Delfosse et al., 2005), on aluminum solubility and release (Dahlgren and Saigusa, 1994; Takahashi et al., 2008), on aluminum toxicity to living beings (Pansombat et al., 1997; Yamada et al., 2011), and on soil productivity (Matsuyama et al., 2005). Notably, most previous studies have considered allophanic Andosols as a whole, without distinguishing the contributions from the different components of the soils individually. As discussed above, acidification-induced alterations of allophanic Andosols should largely depend on the performance of allophane under acidification, given that allophane as a poorly crystalline aluminosilicate should be readily dissolved in acidic conditions. Therefore, how the microstructure of allophane changes during soil acidification is a key to understanding the soil acidification of allophanic Andosols and thereby warrants in-depth investigation. However, so far the studies on the microstructural alterations of allophane and the related mechanisms under acidic conditions are still rare, and most of them are focused on allophane's identification (Higashi and Ikeda, 1974; Pérez et al., 2016), synthesis and purification(Ohashi et al., 2002; Wada, 2011), neoformation (Farmer et al., 1980; Parfitt and Kimble, 1989; Gerard et al., 2007; Li et al., 2020), adsorption of guest species (Nishikiori et al., 2009; Harsh, 2012; Matsuura et al., 2013; Silva-Yumi et al., 2018), and material applications (Toyota et al., 2017; Deng et al., 2019). This situation is partly due to the small particle size and poor crystallinity of allophane, requiring highly challenging analytical techniques.

In the present work, instead of purified natural allophane, synthetic allophane was used in acid leaching experiments to avoid the structural alterations of allophane during purification (Hiradate, 2005). As mentioned above, the pH value of acidified allophanic Andosols could be < 4.0, and that of acid rain near active volcanos could be 2.5 or lower. Six acidic solutions (initial pH = 4.0, 3.5, 3.0, 2.5, 2.2, and 2.0) were used to react with pure allophane for 24 h. The short-term laboratory acidification experiments of allophane are important for predicting the rapid response of allophanic Andosols to peaks of acid inputs. The aims of this study were as follows: i) to identify the chemical and structural stability of allophane under typically acidic conditions and the mechanism of structural changes; ii) to understand the crucial role of allophane in acid buffering capacity and acidification-induced property changes of allophanic Andosols and to gain the implications for soil management. To achieve these objectives, inductively coupled plasma-optical emission spectrometry (ICP-OES), transmission electron microscopy (TEM), X-ray diffraction (XRD), Fourier-transform infrared (FT-IR) spectroscopy, solid-state magic-angle-spinning nuclear magnetic resonance (MAS NMR), and N_2 physisorption analysis were employed.

2. Materials and methods

2.1. Allophane synthesis

Allophane used in this work was hydrothermally synthesized according to Ohashi et al. (2002). The silicon (Si)- and aluminum (Al)-source solutions (0.1 mol/L) were prepared using Na_4SiO_4 (Alfa Aesar) and $AlCl_3{\cdot}6H_2O$ (Sigma-Aldrich), respectively. The precursor gels for the allophane synthesis were prepared by rapid mixing and continuous stirring (for 1 h at room temperature) of Si and Al solutions with a molar ratio of Si/Al = 0.75. Sodium chloride formed as a by-product was removed by centrifugation at the speed of 4000 rpm for 10 min. The white precursors were autoclaved by performing the hydrothermal reaction at 100 °C for 48 h. The resulting materials were dialyzed with ultra-pure water until they came to near-neutral pH. Subsequently, the obtained samples were freeze-dried, ground in a mortar, and denoted as "Allo". The chemical composition of Allo was recognized by XRF and showed a Si/Al molar ratio of 0.77 (Wang et al., 2018). This ratio is between 0.5 and 1.0, indicating that the polymerized silicate could be present in the sample (Parfitt, 1990).

2.2. Batch experiment protocols

A series of dilute acid solutions (initial pH = 4.0, 3.5, 3.0, 2.5, 2.2,

and 2.0) were prepared by using concentrated sulfuric acid (98%, Guangzhou Chemical Reagent Factory, China). Acid leaching experiments of Allo were carried out in a batch system at room temperature. 0.5 g Allo and 200 mL of freshly prepared H_2SO_4 solution were added into a 250 mL polypropylene bottle followed by sealing. Then, they were shaken at a constant rate of 200 r/min for 24 h. After that, 20 mL of saturated sodium chloride solution was injected to the dispersion, sat for 10 min and then centrifuged at 11000*g* for 30 min. The supernatant solutions were used to determine the concentrations of dissolved elements (Si and Al) by Inductively Coupled Plasma-optical Emission Spectrometry (ICP-OES), while the sediments were dialyzed against ultra-pure water until the near-neutral pH was achieved. The resulting products were freeze-dried and then labeled as "$Allo_n$", where n was referred to the initial pH value of the acidic solution. For example, the $Allo_{4.0}$ indicates the acid-leached product in an acidic solution of initial pH = 4.0.

2.3. Characterization methods

The concentrations of dissolved-Si and dissolved-Al in suspensions were analyzed by ICP-OES (Optima 2000DV PerkinElmer, USA). The blank was 2 wt% HNO_3 acidified ultra-pure water. Before measurement, all supernatants were appropriately acidified with 2 wt% HNO_3. For each sample, measurements were repeated three times and the mean value was employed.

TEM with energy-dispersive X-ray (EDX) results were obtained on the FEI Talos F200S field-emission transmission electron microscope operating at 200 kV. The Allo was ultrasonically dispersed in pH 4.0 water for 10 min, and then the as-received dispersion was dropped on a carbon-coated copper grid followed by drying it at ambient condition. For acid-treated products, the specimens were prepared using the dialyzed sediments without freeze-drying.

XRD patterns were recorded on a Bruker D8 Advance diffractometer (Manheim, Germany) with a Ni filter and Cu Kα radiation (λ = 0.154 nm) generated at a voltage of 40 kV and a current of 40 mA. The specimens were investigated from 3° to 70° (2θ) with a scanning rate of 3° (2θ/min).

FT-IR absorbance spectra were recorded using a Bruker Vertex 70 FT-IR spectrometer (Manheim, Germany) with a 4 cm^{-1} spectral resolution. A pure KBr wafer was measured as the background. Each specimen used for FT-IR measurement was prepared by grinding 0.9 mg of sample powder with 80 mg of KBr followed by pressing the mixture into a wafer. All of the spectra were collected over 64 scans in the range of 4000–400 cm^{-1}.

Solid-state MAS NMR spectra were recorded on BRUKER AVANCE III 600 spectrometer (magnetic field 14.1 T) equipped with a 4 mm probe operating at ^{27}Al and ^{29}Si resonance frequencies of 156.4 MHz and 119.2 MHz, respectively. Freeze-dried samples without further treatment were used in the measurements. ^{29}Si MAS NMR spectra were recorded using a contact time of 6 ms, a π/2 pulse length of 2.3 μs, a recycle delay of 2 s, and a spinning rate of 10 kHz. ^{27}Al MAS NMR spectra were recorded using a small-flip angle technique with a pulse length of 0.5 μs (< π/12), a recycle delay of 1 s, and a spinning rate of 14 kHz. The chemical shifts of ^{27}Al and ^{29}Si were referenced to 1 mol/L $Al(NO_3)_3$ and tetramethylsilane (TMS), respectively.

Nitrogen (N_2) physisorption measurements were performed on a Micromeritrics ASAP 2020 system (Norcross, USA) at liquid-nitrogen temperature (T = −196 °C). To completely remove the physically adsorbed water, all samples were degassed at 200 °C for 12 h before analysis. The *SSA* was calculated from nitrogen adsorption data using the Brunauer-Emmett-Teller (BET) method, and the total pore volume (V_{total}) was estimated from the nitrogen uptake at a relative pressure of approximately 0.95 (Thommes et al., 2015). The microporous specific surface area (S_{micro}) and the micropore volume (V_{micro}) were derived from the *t*-plot method; the Barrett-Joyner-Halenda (BJH) method was used to calculate the mesopore volume (V_{meso}) (Lowell et al., 2004).

Table 1
The dissolved proportions of Si and Al from Allo, and the Si/Al molar ratios in suspensions and residual solids calculated using ICP-OES and XRF data.

Sample	Dissolved Si (%)	Dissolved Al (%)	*Dissolved Si/Al	*Residual Si/Al	**$pH_{initial}$	**pH_{end}
Allo	–	–	–	0.77	–	–
$Allo_{4.0}$	0.92	0.04	17.71	0.76	4.0	4.15
$Allo_{3.5}$	1.10	0.13	6.52	0.76	3.5	3.97
$Allo_{3.0}$	2.18	0.70	2.40	0.76	3.0	3.96
$Allo_{2.5}$	4.54	6.35	0.55	0.78	2.5	3.80
$Allo_{2.2}$	8.51	15.26	0.43	0.83	2.2	3.58
$Allo_{2.0}$	11.98	27.57	0.33	0.94	2.0	3.46

*Si/Al Molar ratio.
**The $pH_{initial}$ and pH_{end} refer to the pH value of the initial and terminal supernatants, respectively.

3. Results

3.1. Chemical analysis

As shown in Table 1, both dissolved Si and Al were very low in weakly acidic conditions (initial pH ≥ 3.0) but increased dramatically as the initial pH decreased further. If the dissolution of Allo was unselective or congruent, the dissolved Si/Al ratios could be equal to that of Allo (i.e., Si/Al = 0.77). Nonstoichiometric dissolution occurred in all of the experiments. The proportion of dissolved Si was greater than that of Al at conditions with initial pH ≥ 3.0, while the opposite results were obtained at an initial pH ≤ 2.5. As a result, the Si/Al values of residues decreased at first and then increased. The dissolution of the mineral consumed H^+, thereby increasing the pH value of the terminal supernatants. Even if the onset of the experiment was at pH = 2.0, the pH value of supernatants became mildly acidic (pH_{end} = 3.46) at the end of the reaction.

3.2. TEM-EDX results

As shown in Fig. 1a,b, well-dispersed particles with a ring shape were identified together with some fluffy clusters. The single-particle showed internal and external diameters of approximately 3 nm and 5 nm, respectively. In addition, the poor crystallinity of Allo was also confirmed by selected area electron diffraction (SAED), which only showed wide rings (Fig. 1b inset). These characteristics have been widely reported for hollow spherical allophane, no matter synthetic or natural (Parfitt, 1990; Ohashi et al., 2002). Colloidal silica was not observed, indicating that all the Si atoms were incorporated into Allo. Under conditions with initial pH ≥ 3.0, acid leaching seemed to make no remarkable changes in the morphology of the samples, and the aggregates in products were still fluffy rather than conjoined into large hardened blocks (e.g., Fig. 1c). However, in the case of the initial pH ≤ 2.5, amorphous silica with gel-like morphology was observed, meanwhile, the acid-leached products were severely agglomerated (Fig. 1d–g). Despite that, allophane particles and/or structural fragments remained in $Allo_{2.0}$, as suggested by the fact that some fluffy aggregates were still present and showed a Si/Al ratio close to Allo (point 4# indicated in Fig. 1e and g).

3.3. XRD patterns

The XRD pattern of Allo exhibited one major reflection centered at 3.4 Å and two weak reflections at about 2.3 Å and 1.4 Å (Fig. 2a), which were the typical characteristics for allophane (Harsh, 2012). The former was related to the interference between neighboring SiO tetrahedra; the latter two reflections were also reported in XRD patterns of imogolite, corresponding to the imogolite-like local structure (ImoLS) (Henmi et al., 1981; Du et al., 2017). The boehmite and gibbsite, which generally appeared as by-products (Ohashi et al., 2002), were not observed

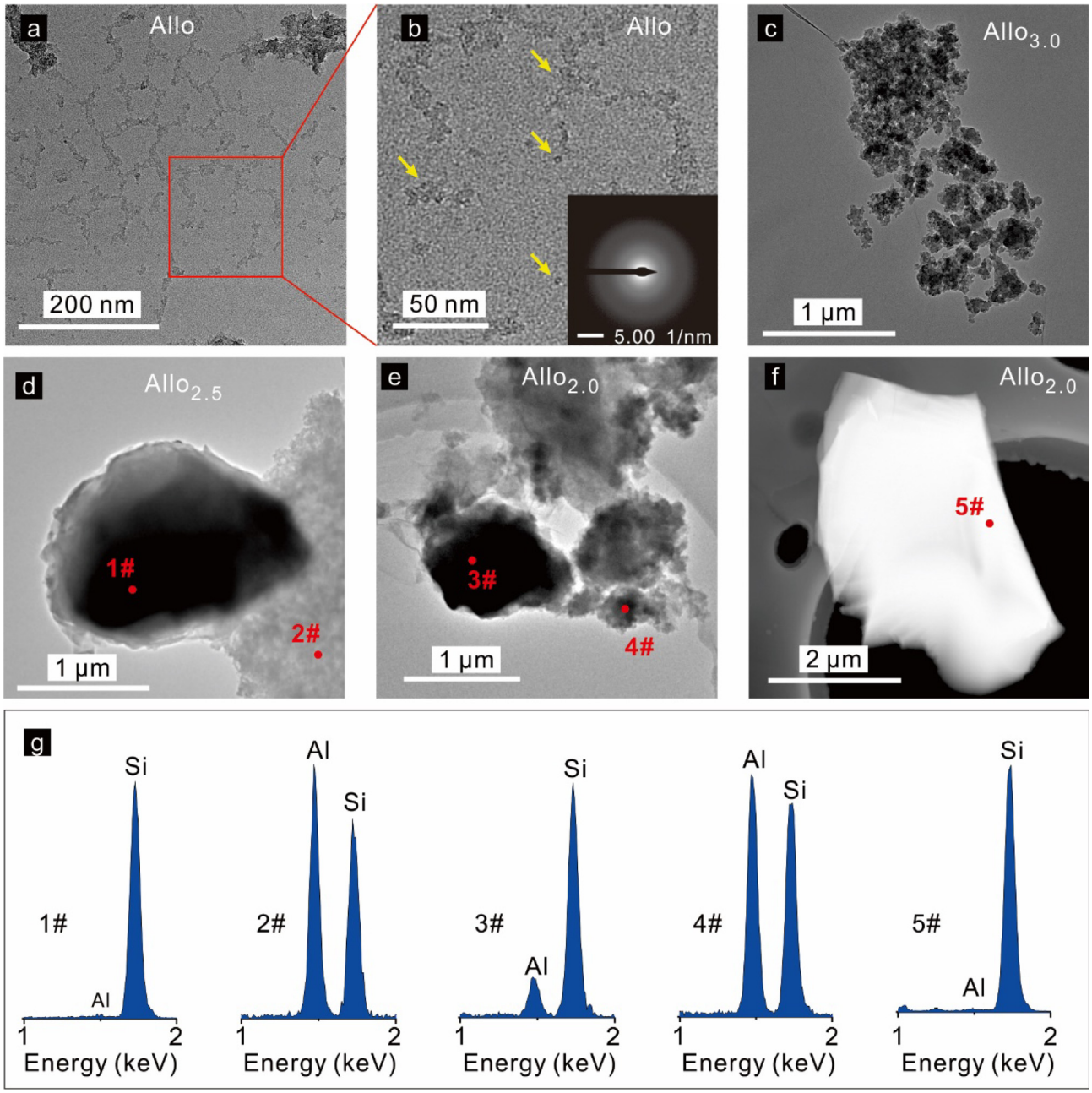

Fig. 1. TEM images and EDX data of Allo and acid-leached products. a–f, TEM images of Allo, $Allo_{3.0}$, $Allo_{2.5}$, and $Allo_{2.0}$, respectively; SAED image of Allo (inset of b); g, EDX data of points 1–5# in d–f. The yellow arrows indicate the hollow spherical particles of allophane.

here, indicating that the Al atoms were incorporated into Allo. As expected, no significant changes were observed in the XRD patterns of the products (e.g., $Allo_{3.0}$) when acid leaching was conducted at conditions with initial pH ≥ 3.0. By contrast, the reflections located at 2.3 and 1.4 Å of $Allo_{2.5}$ began to decrease in their relative intensities, and that of $Allo_{2.0}$ nearly disappeared (Fig. 2c–e), indicating the destruction of ImoLS. Simultaneously, the reflection at 3.4 Å was broadened in its full width at half maximum, which might result from the formation of amorphous silica.

3.4. FTIR spectra

The FTIR spectrum of Allo (Fig. 3a) was in good agreement with that of both natural and synthetic allophane. The most intensive band centered at 982 cm^{-1} was related to the framework of the hollow spherule and was assigned to the Si-O-(Al) stretching vibration. Two shoulder bands at about 1035 and 1140 cm^{-1}, which were ascribed to Si-O-Si stretching vibration with and without tetrahedral Al modification, respectively (Zhou and Zeng, 2017), suggested the presence of polymerized silicates. In the region of 800–400 cm^{-1}, four additional absorption bands that were consistently associated with the lattice vibrations of imogolite were attributed to various vibrations in ImoLS (Parfitt et al., 1980; Wilson et al., 1986; Du et al., 2017). After acid leaching, the most remarkable changes were that the band position of Si-O-(Al) stretching vibration gradually shifted from 982 cm^{-1} to 971 cm^{-1} (Fig. 3b–g). By comparison, no significant changes occurred in the bands located at 680, 590, 505 and 433 cm^{-1}, which might indicate that the residual fragments still consisted of complete and/or nearly complete structural units of ImoLS. In addition, the acid-leached products that were obtained at strongly acidic conditions (pH < 3.0) exhibited a decrease in the relative intensity of the 1035 cm^{-1} band but an increase in that of the 1140 cm^{-1} band (Fig. 3e–g).

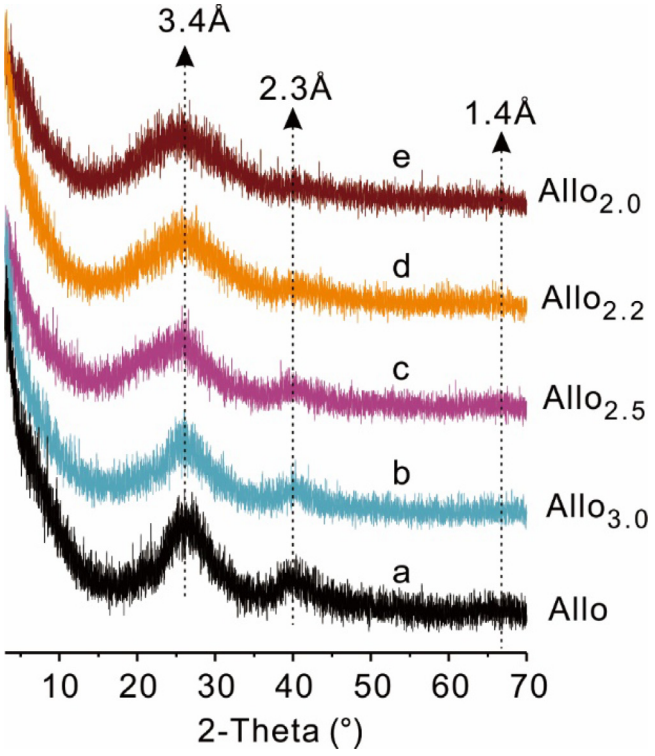

Fig. 2. XRD patterns of Allo and its acid-leached products.

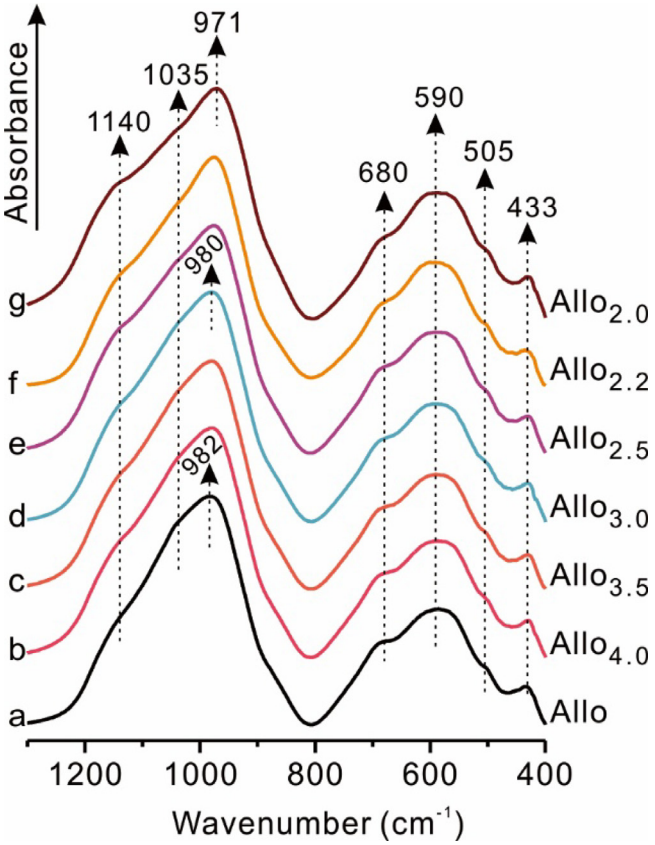

Fig. 3. FT-IR spectra of Allo and its acid-leached products.

3.5. ^{27}Al and ^{29}Si MAS NMR results

As shown in Fig. 4a, two main resonances were observed in all of the spectra of ^{29}Si MAS NMR. The first was the easily identifiable resonance at −78 ppm, as was common in imogolite. It was attributed to $Q^3(6Al)$ coordination, i.e., isolated SiO tetrahedra in ImoLS (Yucelen et al., 2012). Such narrow linewidth indicated the high regularity of the Si coordination environment (Barron et al., 1982). Another broad signal centered at about −90 ppm suggested the presence of amorphous Si species, i.e., polymerized silicates, in which Si atoms were connected with 0–5 next-nearest neighbor Al atoms (Wilson et al., 1986; Du et al., 2017). After acid leaching, the integral area of the broad resonance decreased at first and then increased as the initial pH decreased.

The Al coordination environments were also clarified by the ^{27}Al MAS NMR spectra shown in Fig. 4b. The most pronounced signal at 7.8 ppm was ascribed to the six-coordinated Al (Al^{VI}) in the gibbsite-like sheet of the framework (Hiradate and Wada, 2005), corresponding to −78 ppm in ^{29}Si MAS NMR spectra (Fig. 4a). In addition, an extremely weak resonance located at 34 ppm was assigned to the five-coordinated Al (Al^{V}), which was much pronounced in calcined allophane and that might be associated with the edges of fragments of incomplete octahedral sheets (Childs et al., 1999; Hatakeyama et al., 2011; Du et al., 2018). Another resonance located at 60 ppm was also observed, corresponding to the four-coordinated Al (Al^{IV}). Compared with Allo, acid-leached products showed a smaller integral area of resonance centered at 60 ppm when the initial pH was lower, suggesting that the proportion of Al^{IV} decreased.

3.6. N_2 physisorption analysis

As recommended by the International Union of Pure and Applied Chemistry (IUPAC) (Thommes et al., 2015), the isotherm of Allo resembled a mixture of Type I(b) and IV(a) with an intermediate hysteresis loop between Type H2(b) and H4 (Fig. 5a). Under conditions with initial pH > 3.0, acid leaching made no significant alterations in the isotherms of the products (Fig. 5a–c), but the derived textural parameters increased slightly (Table 2). When acid leaching was conducted at lower initial pH (≤3.0) conditions, the textural parameters of micropores continued to increase, reaching maxima at initial pH = 2.2 (Table 2). In contrast, both the size of the hysteresis loop and the total amount of adsorbed N_2 were reduced (Fig. 5d–g). Correspondingly, the mesopore volume and total pore volume began to decrease in $Allo_{3.0}$. For $Allo_{2.0}$, sharp decreases were observed in all of the textural parameters, implying the serious destruction of hollow spherules. Nevertheless, the values of *SSA* and V_{total} were still as high as 172.1 m^2/g and 0.1206 cm^3/g, respectively, in which the micropores accounted for a large percentage.

4. Discussion

4.1. Acid-induced structural changes and related mechanisms of allophane

The results from this work indicate that the structural changes of Allo are highly dependent on the initial acidity of the input solutions. After leaching in conditions with initial pH < 3.0, profound changes were observed in Allo's chemical composition, microstructure, and porosity. Comparing the structural characteristics of acid-leached products with that of Allo, a conceptual model that involves the acid-induced structural changes of allophane and the related mechanisms is proposed and is illustrated in Fig. 6. Under weakly acidic conditions (initial pH ≥ 3.0), some polymerized silicates are dissolved and some defect pores are enlarged, whereas the framework of the hollow spherule is almost intact. Under strongly acidic conditions (initial pH < 3.0), the dissolution of both polymerized silicates and ImoLS occur, which further enlarge the defect pores or even result in the destruction of hollow spherule. Following the destruction of ImoLS,

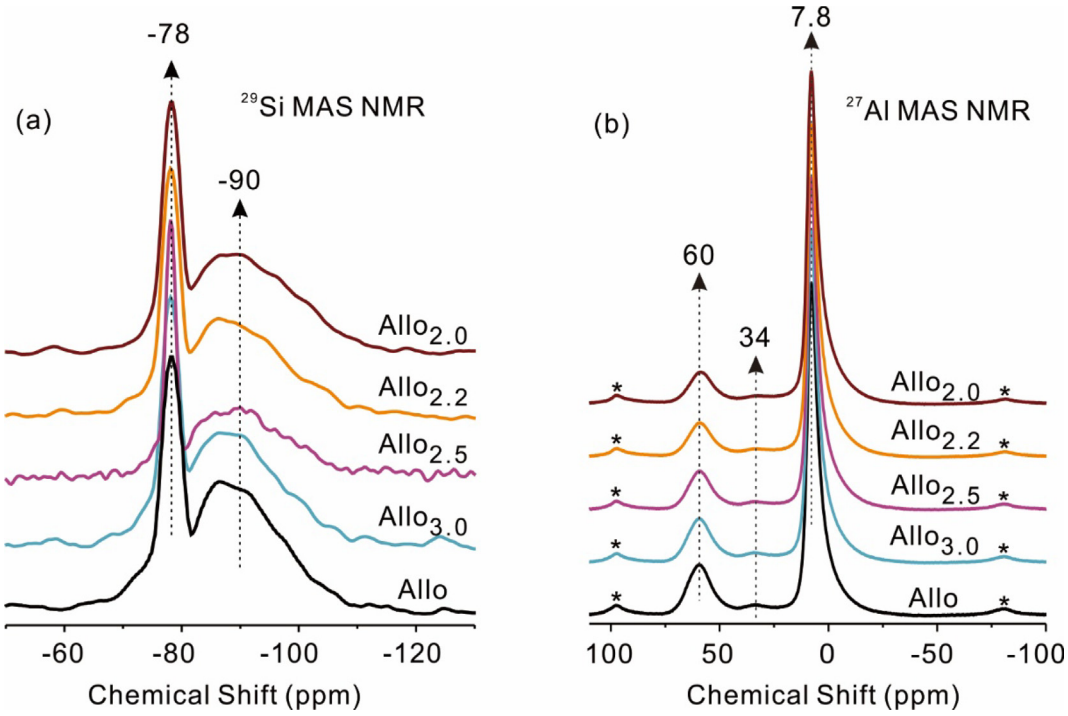

Fig. 4. (a) ^{29}Si MAS NMR and (b) ^{27}Al MAS NMR spectra of Allo and its acid-leached products. Asterisk (*) denotes spinning sideband.

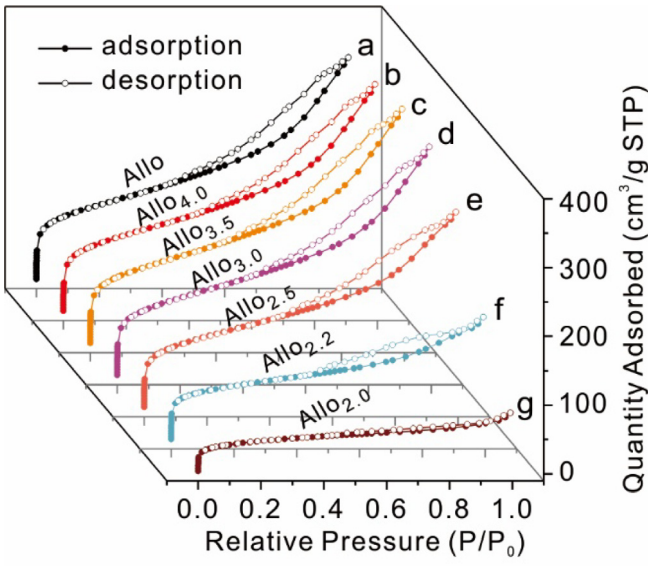

Fig. 5. Nitrogen adsorption–desorption isotherms of Allo and its acid-leached products.

Table 2
Textural parameters derived from the N_2 adsorption–desorption isotherms of Allo and its acid-leached products.

	SSA (m^2/g)	S_{micro} (m^2/g)	$S_{external}$[a] (m^2/g)	V_{total} (cm^3/g)	V_{micro} (cm^3/g)	V_{meso} (cm^3/g)
Allo	399.5	102.2	297.3	0.4694	0.044	0.305
Allo$_{4.0}$	410.2	112.0	298.2	0.4790	0.047	0.312
Allo$_{3.5}$	423.3	112.7	310.6	0.4955	0.048	0.322
Allo$_{3.0}$	417.1	120.6	296.5	0.4816	0.051	0.313
Allo$_{2.5}$	382.3	127.4	254.9	0.4161	0.057	0.215
Allo$_{2.2}$	292.3	161.4	130.9	0.2559	0.071	0.141
Allo$_{2.0}$	172.1	114.0	58.1	0.1206	0.051	0.056

[a] $S_{external} = SSA - S_{micro}$.

amorphous silica is formed. It is worth mentioning that similar structural evolution of allophane has been observed in weakly alkaline conditions in our previous work, and silica-alumina gels are more likely to be formed after the destruction of hollow spherule (Wang et al., 2018).

Specifically, under weakly acidic conditions (initial pH ≥ 3.0), the morphological characteristics of hollow spherical allophane were nearly intact (Fig. 1a–c). The chemical composition of Allo was changed limitedly (Table 1). Some polymerized silicates attached to the framework of Allo might be dissolved, as suggested by the decreased relative intensity of the broad resonance centered at −90 ppm (Fig. 4a). Furthermore, such an assumption is directly confirmed by the shift of 982 cm^{-1} band (Fig. 3a–d), as the position of this band can gradually shift from 970 to 1020 cm^{-1} as the Si/Al molar ratio of allophane increases from 0.5 to 1.0 due to the presence of polymerized silicates attached to the framework (Parfitt et al., 1980; Levard et al., 2012). The proportion of dissolved Si was much larger than that of dissolved Al in leachate solutions (Table 1). Since the substitution of tetrahedral Si by Al often occurs in polymerized silicates (Ildefonse et al., 1994; Yucelen et al., 2012), the main source of dissolved Al should be from the Al^{IV} in polymerized silicates, which is further supported by the decreased relative intensity of the Al^{IV} signal (60 ppm resonance in Fig. 4b). Similar observations are also reported in acid leaching of other aluminosilicates (e.g., smectite and kaolinite), which is attributed to the preferential dissolution of amorphous silica cementing on the mineral surface (Metz et al., 2005).

As reported by Abidin et al. (2007), polymerized silicates commonly appear around the defect pore regions. The removal of polymerized silicates is expected to enlarge the defect pores. The type of the N_2 adsorption–desorption isotherm of Allo (Fig. 5a) confirmed the presence of heterogeneous pores, consisting of micropores (< 2 nm), mesopores (2–50 nm) as well as macropores (> 50 nm). As suggested by Filimonova et al. (2016) and Wang et al. (2018), two main sources of pores are as follows: i) primary pores: voids of hollow spherules (connected with the outside through 0.35–0.5 nm-sized defect pores); and ii) secondary pores: inter-particle and inter-microaggregate spaces (≥0.78 nm, calculated using the ideal hollow spherules with an

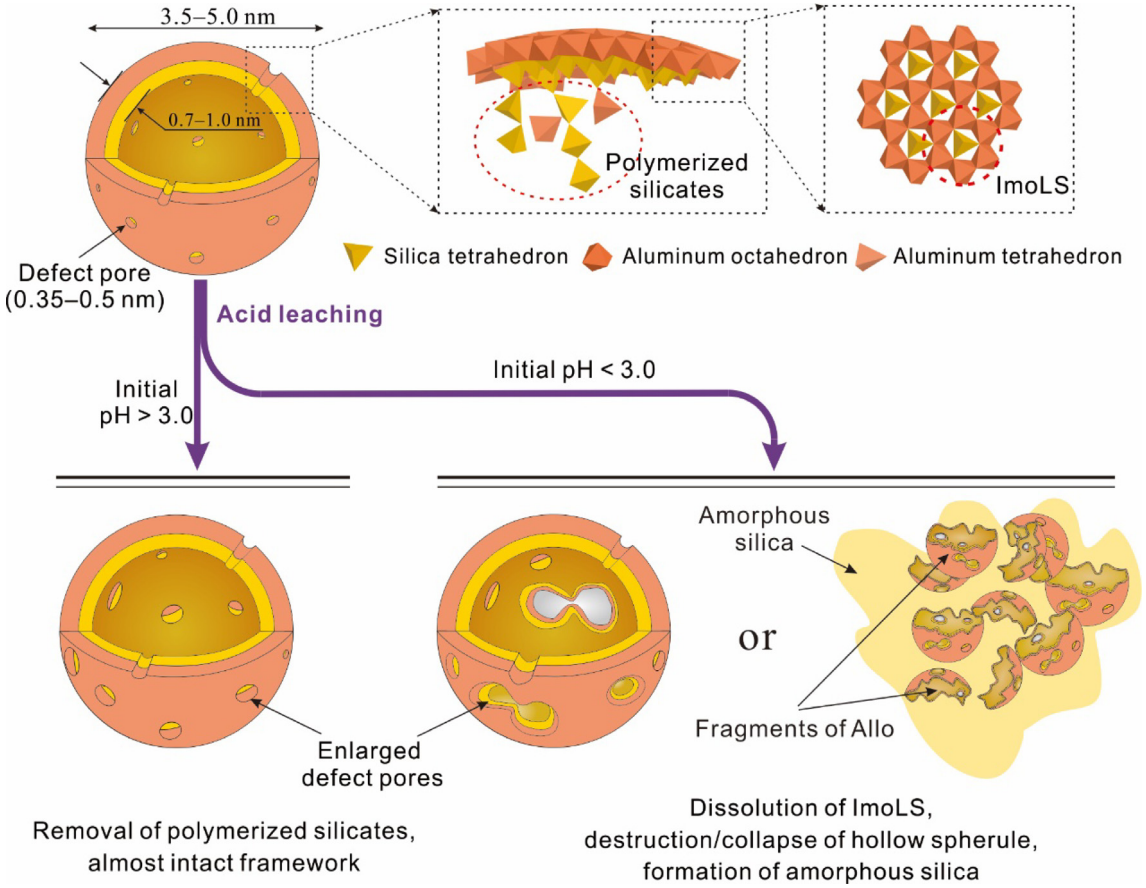

Fig. 6. Structural changes and related mechanisms of allophane under different acidic conditions.

external diameter of 5 nm). Since the N_2 adsorption is kinetically limited in pores of < 0.5 nm in diameter (de Jonge and Mittelmeijer-Hazeleger, 1996), N_2 molecules might fail in well detecting the voids of hollow spherules. However, the dissolution of polymerized silicates is highly probable to make some voids of hollow spherules be detectable by N_2 adsorption, which makes sense for the increases in S_{micro} and V_{micro} (Table 2). When the initial pH value is 3.0, a fringe of hollow spherules may begin to collapse because the textural parameters related to secondary pores showed a slight decrease (Table 2).

Under strongly acidic conditions (initial pH < 3.0), both desilication and dealumination reactions were significantly enhanced, resulting in the dramatic increases in the dissolved proportions of both Si and Al (Table 1). The effect of acidic solutions on the dissolution of Allo can come into play in two ways: via pH effect and SO_4^{2-} effect. On one hand, mineral dissolution in acidic media occurs at the solid-aqueous interfaces. It proceeds by proton adsorption on mineral surface sites followed by hydrolysis, resulting in the release of cations into suspension (Cama et al., 2002; Bibi et al., 2014). As a proton-promoted process, mineral dissolution can be facilitated through decreasing solution pH (i.e., increasing proton concentration). Furthermore, low pH could also promote dissolution reactions by increasing the degree of saturation of the solution (Amram and Ganor, 2005). On the other hand, SO_4^{2-} can strongly bond to the gibbsite-like surface through ligand exchange with aluminol groups (Padilla et al., 2002), which can weaken the bond order between Al and O atoms in the chemical structure of Allo (Henmi et al., 2001). Therefore, the dissolution of Allo can be facilitated.

In addition to the dissolution of polymerized silicates, the destruction of ImoLS also occurs in the above-mentioned initial pH < 3.0 conditions, as indicated by the XRD (Fig. 2c–e) and FTIR results (Fig. 3e–g). Meanwhile, the formation of amorphous silica is indicated by the TEM-EDX results (Fig. 1d–g). Evidence for this statement also arises from the increased proportions of Si–O–Si bonds and disordered Si species, as indicated by the increased relative intensities of 1140 cm^{-1} band and −90 ppm resonance in FTIR spectra (Fig. 3e–g) and ^{29}Si MAS NMR results (Fig. 4a), respectively. As described previously, the dissolution of polymerized silicates can make the Si-O-(Al) bands shift to relatively low wavenumber, however, the newly-formed amorphous silica does not flip this trend in the case of pH ≤ 2.5 (Fig. 3e–g). These results imply that the newly-formed amorphous silica is physically mixed with residual ImoLS. Polymerized silicates are nearly completely removed from Allo after leaching in initial pH = 2.0 conditions, as indicated by the position (971 cm^{-1}) of Si-O-(Al) stretching vibration (Fig. 3g); the edges of ImoLS may contain some Al^{IV} (Hu et al., 2004; Yucelen et al., 2011). Therefore, it is reasonable to conclude that a considerable amount of Al^{IV} still remains in $Allo_{2.0}$ (Fig. 4b).

For aluminosilicates, the dissolution progresses by breaking of bridge oxygen bonds (i.e., Al–OH–Al and Al–O–Si) at the edges as well as at the gibbsite-like surface (Wieland and Stumm, 1992). Furthermore, the dissolution is limited by the breaking of Al–O bonds under acidic conditions because the breaking of the Al–O bond is relatively easy compared to the Si–O bond, no matter for aluminosilicate or simple hydroxides (Huertas et al., 1999; Bibi et al., 2014). Taking the framework structure of allophane into consideration, the SiO tetrahedra within ImoLS would be released following the destruction of the gibbsite-like sheet. That is, the release of Si and Al from ImoLS is (close to) stoichiometric, from which it makes sense that the IR absorption bands (in the range of 800–400 cm^{-1}) ascribed to ImoLS are barely changed (Fig. 3e–g). Hence, the observed non-stoichiometric dissolution in initial pH < 3.0 (Table 1) should result from the formation of amorphous silica.

There is no doubt that the removal of polymerized silicate could enlarge the defect pores, and the defect pore size can be further enlarged following the dissolution of ImoLS along the edges of defect pores. Consequently, many more voids of hollow spherules become detectable by N_2 physisorption, as characterized by the remarkable increases of microporous parameters of acid-treated products, especially in $Allo_{2.2}$. Moreover, the collapse of hollow spherules is expected to be much more common due to the havoc of the framework caused by the ImoLS destruction. The structural fragments together with the newly-formed amorphous silica tend to agglomerate seriously (Fig. 1d,e), causing some secondary pores to disappear. Indeed, all of the mesopore parameters decreased dramatically in the case of pH < 3.0 (Table 2). Nevertheless, some unaltered and/or mildly altered hollow spherules remain in $Allo_{2.0}$, as deduced from the textural parameters.

On the other hand, certain physiochemical properties of allophane could be altered following its structural changes. For example, polymerized silicates in allophane have Si-OH groups that can perform as negative variable surface charges (Okazaki et al., 1989; Henmi et al., 1997; Nartey et al., 2001). Accordingly, the removal of them supposedly makes the isoelectric point (IEP) of products shift to higher pH values. Moreover, the decreases of *SSA* and porosity of allophane resulting from the destruction of hollow spherules may diminish the adsorption and storage capacities of guests.

4.2. Understanding the role of allophane during acidification of allophanic Andosols and implications for soil management

This study depicts the underlying and previously unexplored mechanisms of the alterations of allophane under acidic conditions. Similar processes might also occur in acidified allophanic Andosols. The unraveled changes of allophane under acidic conditions are significant for understanding the acid buffering capacity and evaluating the Al toxicity of allophanic Andosols, and they may guide soil management from a mineralogical perspective as well.

The pH buffering capacity of Andosol is considered as a major factor in controlling soil acidification rates (Shi et al., 2019). Field experiments carried out by Delfosse et al. (2005) found that allophane-rich Andosols exhibit a larger acid-buffering capacity than their non-allophanic counterparts. This feature of allophanic Andosols might be highly related to the high reactivity of allophane. Data presented in Table 1 suggest that allophane is more likely to rapidly respond to the acid inputs and regulate the environmental acidity to mildly acidic or near to neutral state within a short period and that the dissolution of allophane may gradually come to dominate the main mechanism under strongly acidic conditions (e.g., pH < 3.0). These results are in good agreement with the proposal that the major short-term acid buffering mechanisms are the protonation of variable charge sites with subsequent liberation of basic cations and dissolution of sesquioxides (van Breemen et al., 1983), although multiple buffering mechanisms might occur in allophanic Andosols (Matsuyama et al., 2005; Herre et al., 2007).

For the evaluation of Al toxicity, the changes of allophane may provide insight into the sources of active Al of acidified allophanic Andosols. The potassium chloride (KCl)-extractable Al is often used as an indicator of Al toxicity that manifests as adverse effects on the development of Al-susceptible plant roots and the activities of some microorganisms and enzymes (Pansombat et al., 1997; Yamada et al., 2011; Kunito et al., 2016). It is known that the dominant form of active Al in allophanic Andosols is that existing in allophane, and the active Al of this type is not KCl-extractable; the most probable source of KCl extractable Al is from Al-humus complexes (Takahashi et al., 2003; Yamada et al., 2011). In allophanic Andosols, Al-humus complexes might exist but with a low amount (Dahlgren et al., 2004). Therefore, allophanic Andosols commonly contain a very low level of potassium chloride (KCl)-extractable Al. The concentrations of KCl-extractable Al in the local environment would increase once the soils were acidified (Matsuyama et al., 2005). As has been reported previously, Al-humus complexes and allophane are the primary sources of KCl-extractable Al of acidified allophanic Andosols, and the Al-humus complexes could be more easily dissolved than allophane (Takahashi et al., 1995; Yamada et al., 2011). The chemical analysis results presented in Table 1 suggest that allophane probably makes no significant contribution to the Al toxicity of allophanic Andosols in a weakly acidified environment (e.g., pH > 3.0). By contrast, under strongly acidic conditions (e.g., pH < 3.0), the rapid response of allophane may make the solubility and release of Al in acidified allophanic Andosols quickly attain equilibrium and display fast reaction kinetics (Dahlgren and Saigusa, 1994). That is, allophane may significantly contribute to Al toxicity in long-term or seriously acidified allophanic Andosols, except for Al-humus complexes.

Another implication is that the obtained high-resolution structural characteristics of acid-leached products might mineralogically predict the acidification states of allophanic Andosols, and further provide guidance for soil management. The weak acidification of allophanic Andosol supposedly removes some polymerized silicates from allophane, which might slightly shift the IEP of allophanic Andosols to higher pH values; most soil properties that involve allophane structure are highly probable to be barely affected. Hence, it is likely to recover the fertility of weakly acidified allophanic Andosols through soil remediation. According to Huertas et al. (1999), in nature, leaching in strongly acidified conditions or prolonging leaching time in weakly acidified conditions can result in the structural collapse of allophane in allophanic Andosols and the formation of amorphous silica, which could irreversibly break the porous structure of allophanic Andosols, thereby reducing their adsorption capacity, tilth, physical and chemical aspects of fertility, and so on. Combined with the enhancement of Al toxicity, soil productivity may be limited. Therefore, the management of allophanic Andosols should be careful to protect the allophane from structural damage.

Given that allophane-rich Andosols may contain some additional components such as SOM, imogolite, short-range ordered Fe oxyhydroxides, and 2:1 interlayered silicates, the response of allophane to soil acidification is highly probable to be not at same as the pure allophane due to the interactions between allophane and other soil components (Dahlgren et al., 2004). For example, SOM is often strongly bound to allophane through ligand exchange, forming organic-mineral coatings on allophane surface. Moreover, the interaction between allophane and SOM tends to form micro- and macro-aggregates (Harsh et al., 2002). As a result, the H^+ may be prevented from approaching allophane, thereby inhibiting or retarding the response of allophane to acidification. In addition, the protonation of some SOM in soils can consume H^+, thereby lowering the acidity of soil solution, which may protect allophane against destruction as well. In natural soils, allophane often contains some iron (Fe), in the form of structural Fe (Fe substituting for octahedral Al) and/or Fe oxyhydroxide coatings (Kaufhold et al., 2010; Baker et al., 2014). Partly due to the poorly crystalline structure and the fine particle size of allophane, literature reports focused on the Fe-containing allophane are sparse; the effect of the presence of Fe on the structural stability of allophane is not well understood. Recently, Filimonova et al. (2016) reported that the presence of Fe in allophane may increase the proportion of oxidized organics and the protective capacity towards organic matter. From this point, the presence of Fe in allophane may protect allophane from acid leaching. In short, the soil response to acidification should complexly involve multiple chemical equilibria among the aluminosilicate components (partly associated with organic matter) within these Andosols, and further investigations are required for an in-deeper understanding of the effect of other soil components on the response of allophane to acidification.

5. Conclusion

The structural stability of allophane under moderately and strongly acidic conditions was investigated, filling several knowledge gaps in the field. The structure of allophane exhibited relatively low stability in acidic conditions. Under conditions with initial pH > 3.0, acid leaching only removed some polymerized silicates attached to ImoLS of allophane, but in stronger acidic conditions (pH < 3.0), the destruction of ImoLS also occurred. In the former case, the microporous parameters increased slightly as a result of the enlargement of defect pores. In the latter case, much more Al and Si were released into suspensions. Meanwhile, further enlargement of defect pores and/or collapse of hollow spherules occurred followed by the formation of amorphous silica, which made the products aggregate seriously and become more disordered. These changes damaged the porous structure of allophane, thereby reducing its adsorption and storage capacities to guest species. Note that although all the textural parameters of $Allo_{2.0}$ decreased dramatically, some unaltered and/or mildly altered hollow spherules were still present.

These findings are expected to provide insight into the pH buffering capacity and the sources of Al toxicity of allophanic Andosols and to serve as a guide to soil management from a mineralogical perspective. The quick response and high neutralization capacity of allophane to acid inputs may indicate that allophane is more like to play a significant role in controlling the pH of soil solutions of allophanic Andosols. Since allophane is metastable in acidic conditions, the structural destruction of allophane, in addition to the de-complexation of Al-humus complexes, is more likely to greatly contribute to Al toxicity in the long-term or serious acidification of allophanic Andosols. Furthermore, the porous structure of allophanic Andosols is supposed to be damaged. Hence, prudent management measures should be employed to avoid the structural destruction of allophane to maintain soil productivity. Moreover, weakly acidified allophanic Andosols, in which the structure of allophane is expected to be rarely affected, are highly probable to have their fertility restored through soil remediation.

Declaration of Competing Interest

The authors declare that they have no known competing financial interests or personal relationships that could have appeared to influence the work reported in this paper.

Acknowledgments

Financially supported by the National Natural Science Foundation of China (Grant No. 41672042 and 41972045), Science and Technology Planning Project of Guangdong Province, China (Grant No. 2017B020237003), National Special Support for High-Level Personnel, China, Natural Science Foundation of Guangdong Province, China (Grant No. 2019A1515011957), and China Postdoctoral Science Foundation (Grant No. 2019M653104) are gratefully acknowledged. This is a contribution No. IS-2881 from GIGCAS.

References

Abidin, Z., Matsue, N., Henmi, T., 2006. Validity of proposed model for the chemical structure of allophane with nano-ball morphology. Clay Sci. 12 (S2), 267–269.
Abidin, Z., Matsue, N., Henmi, T., 2007. Nanometer-scale chemical modification of nano-ball allophane. Clay. Clay Miner. 55 (4), 443–449.
Amram, K., Ganor, J., 2005. The combined effect of pH and temperature on smectite dissolution rate under acidic conditions. Geochim. Cosmochim. Acta 69 (10), 2535–2546.
Baker, L.L., Nickerson, R.D., Strawn, D.G., 2014. XAFS study of Fe-substituted allophane and imogolite. Clay. Clay Miner. 62, 20–34.
Barron, P.F., Wilson, M.A., Campbell, A.S., Frost, R.L., 1982. Detection of imogolite in soils using solid-state ^{29}Si NMR. Nature 299 (5884), 616–618.
Bibi, I., Singh, B., Silvester, E., 2014. Dissolution kinetics of soil clays in sulfuric acid solutions: Ionic strength and temperature effects. Appl. Geochem. 51, 170–183.
Cama, J., Metz, V., Ganor, J., 2002. The effect of pH and temperature on kaolinite dissolution rate under acidic conditions. Geochim. Cosmochim. Acta 66 (22), 3913–3926.
Chevallier, T., Woignier, T., Toucet, J., Blanchart, E., 2010. Organic carbon stabilization in the fractal pore structure of Andosols. Geoderma 159 (1–2), 182–188.
Childs, C.W., Hayashi, S., Newman, R.H., 1999. Five-coordinate aluminum in allophane. Clay. Clay Miner. 47 (1), 64–69.
Dahlgren, R.A., Saigusa, M., 1994. Aluminum release rates from allophanic and non-allophanic Andosols. Soil Sci. Plant Nutr. 40 (1), 125–136.
Dahlgren, R.A., Saigusa, M., Ugolini, F.C., 2004. The nature, properties and management of volcanic soils. Adv. Agron. 82, 113–182.
de Jonge, H., Mittelmeijer-Hazeleger, M.C., 1996. Adsorption of CO_2 and N_2 on soil organic matter: nature of porosity, surface area, and diffusion mechanisms. Environ. Sci. Technol. 30 (2), 408–413.
Delfosse, T., Delmelle, P., Iserentant, A., Delvaux, B., 2005. Contribution of SO_3 to the acid neutralizing capacity of Andosols exposed to strong volcanogenic acid and SO_2 deposition. Eur. J. Soil Sci. 56, 113–125.
Delmelle, P., Stix, J., Bourque, C.P.A., Baxter, P.J., Garcia-Alvarez, J., Barquero, J., 2001. Dry deposition and heavy acid loading in the vicinity of Masaya Volcano, a major sulfur and chlorine source in Nicaragua. Environ. Sci. Technol. 35 (7), 1289–1293.
Deng, L.L., Du, P.X., Yu, W.B., Yuan, P., Annabi-Bergaya, F., Liu, D., Zhou, J.M., 2019. Novel hierarchically porous allophane/diatomite nanocomposite for benzene adsorption. Appl. Clay Sci 168, 155–163.
Du, P.X., Yuan, P., Liu, D., Wang, S., Song, H.Z., Guo, H.Z., 2018. Calcination-induced changes in structure, morphology, and porosity of allophane. Appl. Clay Sci 158, 211–218.
Du, P.X., Yuan, P., Thill, A., Annabi-Bergaya, F., Liu, D., Wang, S., 2017. Insights into the formation mechanism of imogolite from a full-range observation of its sol-gel growth. Appl. Clay Sci 150, 115–124.
Farmer, V.C., Russell, J.D., Berrow, M.L., 1980. Imogolite and proto-imogolite allophane in spodic horizons—evidence for a mobile aluminum silicate complex in podzol formation. J. Soil Sci. 31, 673–684.
Filimonova, S., Kaufhold, S., Wagner, F.E., Haeusler, W., Koegel-Knabner, I., 2016. The role of allophane nano-structure and Fe oxide speciation for hosting soil organic matter in an allophanic Andosol. Geochim. Cosmochim. Acta 180, 284–302.
Gerard, M., Caquineau, S., Pinheiro, J., Stoops, G., 2007. Weathering and allophane neoformation in soils developed on volcanic ash in the Azores. Eur. J. Soil Sci. 58, 496–515.
Gonzalez-Rodriguez, S., Fernandez-Marcos, M.L., 2018. Phosphate sorption and desorption by two contrasting volcanic soils of equatorial Africa. PeerJ 6, e5820.
Guo, J.H., Liu, X.J., Zhang, Y., Shen, J.L., Han, W.X., Zhang, W.F., Christie, P., Goulding, K.W.T., Vitousek, P.M., Zhang, F.S., 2010. Significant acidification in major Chinese croplands. Science 327 (5968), 1008–1010.
Harsh, J., 2012. Poorly crystalline aluminosilicate clay minerals, in: Y.L. Pan M.H., Li, Y. C., Sumner, M.E. (Eds.), Handbook of Soil Sciences, second ed. CRC Press, Florida, pp. 23-1–233-13.
Harsh, J., Chorover, J., Nizeyimana, E., 2002. Allophane and imogolite. In: Dixon, J.B., Schulze, D.G. (Eds.), Soil Mineralogy With Environmental Applications. Soil Science Society of America, Madison, pp. 291–322.
Hatakeyama, M., Hara, T., Ichikuni, N., Shimazu, S., 2011. Characterization of heat-treated synthetic imogolite by ^{27}Al MAS and ^{27}Al MQMAS solid-state NMR. Bull. Chem. Soc. Jpn. 84 (6), 656–659.
Henmi, I., Matsue, N., Henmi, T., 2001. Effect of acid species and co-existing anions on the dissolution of Al and Si from allophane by treatment of diluted acid solutions. J. Clay Sci. Soc. Jpn. 2, 58–63.
Henmi, T., Matsue, N., Johan, E., 1997. Change in the surface acidity of allophane with a low Si/Al ratio by reaction with ortho-silicic acid. Jpn. J. Soil Sci. Plant Nutr. 68, 514–520.
Henmi, T., Tange, K., Minagawa, T., Yoshinaga, N., 1981. Effect of SiO_2/Al_2O_3 ratio on the thermal reactions of allophane. II. Infrared and X-ray powder diffraction data. Clay. Clay Miner. 29 (2), 124–128.
Henmi, T., Wada, K., 1976. Morphology and composition of allophane. Am. Mineral. 61, 379–390.
Herre, A., Lang, F., Siebe, C., Dohrmann, R., Kaupenjohann, M., 2007. Mechanisms of acid buffering and formation of secondary minerals in vitric Andosols. Eur. J. Soil Sci. 58 (2), 431–444.
Higashi, T., Ikeda, H., 1974. Dissolution of allophane by acid oxalate solution. Clay Sci. 4, 205–211.
Hiradate, S., 2005. Structural changes of allophane during purification procedures as determined by solid-state ^{27}Al and ^{29}Si NMR. Clay. Clay Miner. 53 (6), 653–658.
Hiradate, S., Wada, S.I., 2005. Weathering process of volcanic glass to allophane determined by ^{27}Al and ^{29}Si solid-state NMR. Clay. Clay Miner. 53 (4), 401–408.
Hu, J., Kannangara, G.S.K., Wilson, M.A., Reddy, N., 2004. The fused silicate route to protoimogolite and imogolite. J. Non-Cryst. Solids 347 (1–3), 224–230.
Huertas, F.J., Chou, L., Wollast, R., 1999. Mechanism of kaolinite dissolution at room temperature and pressure Part II: Kinetic study. Geochim. Cosmochim. Acta 63 (19–20), 3261–3275.
Ildefonse, P., Kirkpatrick, R.J., Montez, B., Calas, G., Flank, A.M., Lagarde, P., 1994. ^{27}Al MAS NMR and aluminum X-ray absorption near edge structure study of imogolite and allophane. Clay. Clay Miner. 42 (3), 276–287.
Johnson, N., Parnell, R.A., 1986. Composition, distribution and neutralization of “acid rain” derived from Masaya volcano. Nicaragua. Tellus B 38 (2), 106–117.
Kaufhold, S., Ufer, K., Kaufhold, A., Stucki, J.W., Anastacio, A.S., Jahn, R., Dohrmann, R., 2010. Quantification of allophane from Ecuador. Clay. Clay Miner. 58, 707–716.
Kelliher, F.M., Parfitt, R.L., van Koten, C., Schipper, L.A., Rys, G., 2013. Use of shallow samples to estimate the total carbon storage in pastoral soils. New Zeal. J. Agr. Res.

56 (1), 86–90.
Khan, H., Matsue, N., Henmi, T., 2006. Adsorption of water on nano-ball allophane. Clay Sci. 12 (S2), 261–266.
Kunito, T., Isomura, I., Sumi, H., Park, H.-D., Toda, H., Otsuka, S., Nagaoka, K., Saeki, K., Senoo, K., 2016. Aluminum and acidity suppress microbial activity and biomass in acidic forest soils. Soil Biol. Biochem. 97, 23–30.
Levard, C., Basile-Doelsch, I., 2016. Geology and mineralogy of imogolite-type materials. In: Yuan, P., Thill, A., Bergaya, F. (Eds.), Nanosized Tubular Clay Minerals: Halloysite and Imogolite. Elsevier, Amsterdam, pp. 49–65.
Levard, C., Doelsch, E., Basile-Doelsch, I., Abidin, Z., Miche, H., Masion, A., Rose, J., Borschneck, D., Bottero, J.Y., 2012. Structure and distribution of allophanes, imogolite and proto-imogolite in volcanic soils. Geoderma 183, 100–108.
Li, Z.M., Cornelis, J.T., Vander Linden, C., Van Ranst, E., Delvaux, B., 2020. Neoformed aluminosilicate and phytogenic silica are competitive sinks in the silicon soil-plant cycle. Geoderma 368, 1–14.
Lowell, S., Shields, J.E., Thomas, M.A., Thommes, M., 2004. Characterization of porous solids and powders: Surface area, pore size and density. Springer, Netherlands.
Matsuura, Y., Iyoda, F., Arakawa, S., John, B., Okamoto, M., Hayashi, H., 2013. DNA adsorption characteristics of hollow spherule allophane nano-particles. Mat. Sci. Eng C-Mater. 33 (8), 5079–5083.
Matsuyama, N., Saigusa, M., Sakaiya, E., Tamakawa, K., Oyamada, Z., Kudo, K., 2005. Acidification and soil productivity of allophanic Andosols affected by heavy application of fertilizers. Soil Sci. Plant Nutr. 51 (1), 117–123.
Metz, V., Amram, K., Ganor, J., 2005. Stoichiometry of smectite dissolution reaction. Geochim. Cosmochim. Acta 69 (7), 1755–1772.
Montarges-Pelletier, E., Bogenez, S., Pelletier, M., Razafitianamaharavo, A., Ghanbaja, J., Lartiges, B., Michot, L., 2005. Synthetic allophane-like particles: Textural properties. Colloid. Surface. A 255 (1), 1–10.
Nanzyo, M., Shoji, S., Dahlgren, R., 1993. Physical characteristics of volcanic ash soils. In: Shoji, S., Nanzyo, M., Dahlgren, R. (Eds.), Volcanic Ash Soils: Genesis, Properties and Utilization. Elsevier, Amsterdam, pp. 189–207.
Nartey, E., Matsue, N., Henmi, T., 2001. Charge characteristics modification mechanisms of nano-ball allophane upon orthosilicic acid adsorption. Clay Sci. 11, 465–477.
Nishikiori, H., Shindoh, J., Takahashi, N., Takagi, T., Tanaka, N., Fujii, T., 2009. Adsorption of benzene derivatives on allophane. Appl. Clay Sci. 43, 160–163.
Ohashi, F., Wada, S.-I., Suzuki, M., Maeda, M., Tomura, S., 2002. Synthetic allophane from high-concentration solutions: nanoengineering of the porous solid. Clay Miner. 37 (3), 451–456.
Okazaki, M., Kimiwada, K., Katsumata, H., 1989. Adsorption of ions on synthetic amorphous aluminosilicates with different SiO_2/Al_2O_3 molar ratios and coordination numbers of aluminum. Soil Sci. Plant Nutr. 35 (1), 109–118.
Padilla, G.N., Matsue, N., Henmi, T., 2002. Change in surface charge properties of nano-ball allophane as influenced by sulfate adsorption. Clay Sci. 12, 33–39.
Pansombat, K., Kanazawa, S., Horiguchi, T., 1997. Microbial ecology in tea soils. Soil Sci. Plant Nutr. 43 (2), 317–327.
Parfitt, R.L., 1990. Allophane in New Zealand-a review. Aust. J. Soil Res. 28 (3), 343–360.
Parfitt, R.L., 2009. Allophane and imogolite: role in soil biogeochemical processes. Clay Miner. 44 (1), 135–155.
Parfitt, R.L., Furkert, R.J., Henmi, T., 1980. Identification and structure of two types of allophane from volcanic ash soils and tephra. Clay. Clay Miner. 28 (5), 328–334.
Parfitt, R.L., Kimble, J.M., 1989. Conditions for formation of allophane in soils. Soil Sci. Soc. Am. J. 53, 971–977.
Parfitt, R.L., Yuan, G., Theng, B.K.G., 1999. A ^{13}C-NMR study of the interactions of soil organic matter with aluminium and allophane in podzols. Eur. J. Soil Sci. 50 (4), 695–700.
Pereira, R.C., Arbestain, M.C., Kelliher, F.M., Theng, B.K.G., McNally, S.R., Macias, F., Guitian, F., 2019. Assessing the pore structure and surface area of allophane-rich and non-allophanic topsoils by supercritical drying and chemical treatment. Geoderma 337, 805–811.
Pérez, N.A., Bucio, L., Lima, E., Soto, E., Cedillo, C., 2016. Identification of allophane and other semi-crystalline and amorphous phases on pre-Hispanic Mexican adobe earth bricks from Cholula. Mexico. Microchem. J. 126, 349–358.
Shi, R.Y., Liu, Z.D., Li, Y., Jiang, T., Xu, M., Li, J.Y., Xu, R.K., 2019. Mechanisms for increasing soil resistance to acidification by long-term manure application. Soil Till. Res. 185, 77–84.
Shoji, S., Nanzyo, M., Dahlgren, R., 1993. Volcanic ash soils: genesis, properties and utilization. Elsevier, Amsterdam.
Silva-Yumi, J., Escudey, M., Gacitua, M., Pizarro, C., 2018. Kinetics, adsorption and desorption of Cd(II) and Cu(II) on natural allophane: effect of iron oxide coating. Geoderma 319, 70–79.
Stevens, K.F., Vucetich, C.G., 1985. Weathering of upper quaternary tephras in New-Zealand: 2. Clay minerals and their climatic interpretation. Chem. Geol. 53 (3–4), 237–247.
Takahashi, T., Fukuoka, T., Dahlgren, R.A., 1995. Aluminum solubility and release rates from soil horizons dominate by aluminum-humus complexes. Soil Sci. Plant Nutr. 41 (1), 119–131.
Takahashi, T., Mitamura, A., Ito, T., Ito, K., Nanzyo, M., Saigusa, M., 2008. Aluminum solubility of strongly acidified allophanic Andosols from Kagoshima Prefecture, southern Japan. Soil Sci. Plant Nutr. 54 (3), 362–368.
Takahashi, T., Sato, T., Sato, A., Nanzyo, M., 2003. Relationship between 1 M KC1-extractable aluminum and pyrophosphate-extractable aluminum in A horizons of non-allophanic Andosols. Soil Sci. Plant Nutr. 49, 729–733.
Takamatsu, T., Boratynski, J., Satake, K., 1992. Effects of volcanic acid deposition on soil chemistry: 1. Status of exchangeable cations and sulfur. Soil Sci. 154 (6), 435–449.
Tao, L., Li, F.B., Liu, C.S., Feng, X.H., Gu, L.L., Wang, B.R., Wen, S.L., Xu, M.G., 2019. Mitigation of soil acidification through changes in soil mineralogy due to long-term fertilization in southern China. Catena 174, 227–234.
Thommes, M., Kaneko, K., Neimark, A.V., Olivier, J.P., Rodriguez-Reinoso, F., Rouquerol, J., Sing, K.S.W., 2015. Physisorption of gases, with special reference to the evaluation of surface area and pore size distribution (IUPAC Technical Report). Pure Appl. Chem. 87 (9–10), 1051–1069.
Toyota, Y., Okamoto, M., Arakawa, S., 2017. New opportunities for drug delivery carrier of natural allophane nanoparticles on human lung cancer A549 cells. Appl. Clay Sci 143, 422–429.
van Breemen, N., Mulder, J., Driscoll, C.T., 1983. Acidification and alkalinization of soils. Plant Soil 75 (3), 283–308.
Wada, K., 1989. Allophane and imogolite. In: Dixon, J.B., Weed, S.B. (Eds.), Minerals in Soil Environments. Soil Sci. Soc. Am, Madison, pp. 1051–1087.
Wada, S.I., 2011. A procedure for separation and purification of allophane from weathered pumice. J. Clay Sci. Soc. Jpn. 40 (4), 242–248.
Wang, S., Du, P.X., Yuan, P., Zhong, X.M., Liu, Y.Q., Liu, D., Deng, L.L., 2018. Changes in the structure and porosity of hollow spherical allophane under alkaline conditions. Appl. Clay Sci 166, 242–249.
Wieland, E., Stumm, W., 1992. Dissolution kinetics of kaolinite in acidic aqueous solutions at 25°C. Geochim. Cosmochim. Acta 56 (9), 3339–3355.
Wilson, M., McCarthy, S., Fredericks, P., 1986. Structure of poorly ordered aluminosilicates. Clay Miner. 21 (5), 879–897.
Woignier, T., Duffours, L., Colombel, P., Dieudonne, P., 2015. Nanoporous clay with carbon sink and pesticide trapping properties. Eur. Phys. J-Spec. Top. 224 (9), 1945–1962.
Yamada, K., Ito, K., Takahashi, T., Kanno, H., Nanzyo, M., 2011. Inhibitory effect of acid Andosols on plants is aluminum toxicity true for allophanic Andosols? Soil Sci. Plant Nutr. 57 (4), 491–499.
Yucelen, G.I., Choudhury, R.P., Leisen, J., Nair, S., Beckham, H.W., 2012. Defect structures in aluminosilicate single-walled nanotubes: A solid-state nuclear magnetic resonance investigation. J. Phys. Chem. C 116 (32), 17149–17157.
Yucelen, G.I., Choudhury, R.P., Vyalikh, A., Scheler, U., Beckham, H.W., Nair, S., 2011. Formation of single-walled aluminosilicate nanotubes from molecular precursors and curved nanoscale intermediates. J. Am. Chem. Soc. 133 (14), 5397–5412.
Zhou, Y., Zeng, H.C., 2017. Synthesis, self-assembly, transformation, and functionalization of nanoscale artificial allophane spherules for catalytic applications. Chem. Mater. 29 (14), 6076–6086.